Comparison of Calculated with Measured Dynamic Aperture*

F. Zimmermann

Stanford Linear Accelerator Center, Stanford, CA 94309, USA

Abstract

The measured dynamic aperture of the HERA proton ring and the value expected from simulation studies agree within a factor of 2. A better agreement is achieved if a realistic tune modulation is included in the simulation. The approximate threshold of tune-modulation induced diffusion can be calculated analytically. Its value is in remarkable agreement with the dynamic aperture measured. The calculation is based on parameters of resonances through order 11 which are computed using differential-algebra methods and normal-form algorithms. Modulational diffusion in conjunction with drifting machine parameters appears to be the most important transverse diffusion process.

1 INTRODUCTION

Dynamic aperture and transverse particle diffusion rates are an important concern in the design and operation of large hadron storage rings. At injection energy, nonlinear persistent-current field errors in the superconducting magnets limit the dynamic aperture of the HERA proton ring, which is the second superconducting storage ring in operation. In this report, simulation studies and an analytical estimate of the dynamic aperture are compared with observations from the first two years of operation.

Section 2 describes the model of HERA used in the simulation and techniques of tracking data analysis. Section 3 is devoted to a comparison of the dynamic aperture measured with that expected from tracking. An analytical study of high-order resonances in the presence of tune modulation and an approach to calculate amplitude-dependent diffusion rates are discussed in Section 4. The results are summarized and some conclusions are drawn in Section 5. This report focuses on the main ideas. For more details see [1, 2, 3].

2 TRACKING SIMULATIONS

2.1 Model of HERA

The main circuit of the HERA proton ring comprises about 400 superconducting dipole magnets and 200 s.c. quadrupoles. A single FODO cell contains four dipoles and has a length of 47 m. Quadrupole and sextupole corrections coils are wound upon the beam pipe along 2/3 of

the length of each dipole to control tune and chromaticity [4]. Every second dipole magnet is equipped with a decapole correction coil, and dodecapole correctors are installed inside the main quadrupoles to locally compensate the largest systematic multipole components [5].

The normal and skew multipole components through 32-poles have been measured for each of the s.c. HERA magnets. In the simulation, the individual multipole components up to 20-poles of all s.c. dipoles and quadrupoles are taken into account by five thin, higher-order lenses in each FODO half cell. The strengths of the 6-, 10- and 12-pole correctors, independently powered in each quadrant, are added to the individual multipole coefficients of a magnet. This model of HERA is a very good approximation to the real machine.

2.2 Early Indicators of Unstable Trajectories

The minimum time needed to inject 210 bunches into the HERA proton ring is about 20 minutes, corresponding to $6 \cdot 10^7$ turns. A typical number of turns in the tracking studies is 10^4, which requires about 15 minutes CPU time on an IBM 9000-720, using the computer codes RACETRACK and SIXTRACK [6]. Reliable criteria for early detection of unstable trajectories are, therefore, indispensable. A promising method consists of determining the rate of divergence of two initially close trajectories in phase space [7], which is characterized by the Lyapunov exponent and is a well established concept in the theory of nonlinear dynamics [8]. A trajectory is either regular or chaotic. For regular motion the distance d in phase space between two tracks grows linearly with the number of turns N:

$$d(N) \propto N, \qquad (1)$$

when averaged over long periods of time. Chaotic motion is characterized by an exponential growth of this distance:

$$d(N) \propto e^{\lambda N}, \qquad (2)$$

where λ is the Lyapunov exponent. Its formal definition is

$$\lambda \equiv \lim_{N \to \infty} \lim_{d(0) \to 0} \frac{1}{N} \ln \frac{d(N)}{d(0)}. \qquad (3)$$

The main reason for the calculation of Lyapunov exponents in tracking studies is that chaotic particles are potentially unstable and may experience an amplitude growth on a longer time scale. An amplitude increase for chaotic trajectories, and only for those, has indeed been found over a 10–100 times larger number of turns [1].
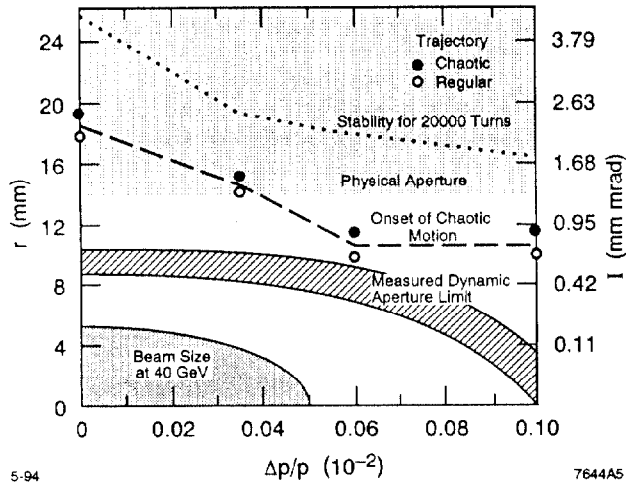
Figure 1: Dynamic aperture in the HERA proton ring: the dynamic aperture r expected from simulation studies, $r \equiv (2\beta(I_x + I_z))^{\frac{1}{2}}$ with $\beta = 76$ m, as a function of the amplitude of momentum oscillations $\Delta p/p$, the two-sigma beam size, and the actual dynamic aperture. The range depicted for the latter refers to the variation observed over periods of days or weeks.

3 PREDICTED AND MEASURED DYNAMIC APERTURE

The predicted and the measured dynamic aperture of the HERA proton ring are shown in Fig. 1, as a function of the amplitude of momentum oscillation $\Delta p/p$. The upper dotted line represents the border above which particles are lost within $2 \cdot 10^4$ turns in the simulation. The amplitude at which the onset of chaotic particle motion is detected by the Lyapunov exponent method using 10^4 turns is about 30 % smaller (18 mm at $\beta = 76$ m for $\Delta p/p \approx 0$). This amplitude was supposed to give a conservative estimate of the actual dynamic aperture.

In 1991/92, the physical aperture, determined by means of orthogonal orbit bumps, was about 14 mm ($\beta = 76$ mm). Beam profile measurements with the residual gas monitors [9], performed after bad injection or excitation, show that the dynamic aperture is only 8.5–11 mm and, hence, is considerably smaller than both the physical aperture and the value expected from the simulation (see Fig. 1). It turned out to be sufficient for stable beam operation.

While measurement and prediction agree within a factor of 2, their difference is too large to be explained by uncertainties in the field errors, beam orbits, and the like. Rather, the difference indicates that some physical effect has been omitted in the simulation.

Two effects that have not been considered are tune modulation and slow drifts of parameters. Current ripple in the superconducting main circuit causes a tune modulation of frequency 50 Hz and of amplitude $5 \cdot 10^{-5}$–10^{-4} (quoted in units of the revolution frequency 47 kHz) [1]. Figure 1 indicates a strong impact of longitudinal oscillations on the dynamic aperture. The effect of synchrotron oscillations

and nonzero chromaticity can to first order be understood by the accompanying tune modulation in the transverse phase space. A typical modulation amplitude amounts to $2 \cdot 10^{-4}$, and the synchrotron frequency is about 20 Hz.

When in addition to the nonlinear field errors a realistic tune modulation (of amplitude $q \approx 10^{-4}$ at a frequency of 50 Hz as that due to magnet current ripple) is also included in the simulation model, the dynamic aperture for on-momentum particles is considerably reduced [1], and chaotic trajectories are found close to the actual dynamic aperture. In this case, the chaotic trajectories at amplitudes between 10 and 16 mm are interspersed among regular regions of phase space, so that tune modulation alone is not sufficient to cause a loss of all particles in this amplitude range. To account for the latter, additional slow drifts of the machine parameters are required which alter the position of chaotic regions in phase space and thereby convert previously regular particles into chaotic ones and vice versa. A continuous drift of parameters is caused, for instance, by low-frequency quadrupole vibrations, by the spread of persistent-current sextupole decay [10] and by temperature changes of magnets and power supplies. From Fig. 2 a tune change by 10^{-4} causes a position change of resonances and chaotic regions in phase space by $|\Delta I_{x,z}| \sim 0.02$ mm mrad ($I_{x,z}$ is the action variable). Neither the total impact of low-frequency tune modulation or synchrotron oscillations, nor the additional effect of parameter drifts can be reliably estimated by tracking studies for 10^4 turns. Here, an analytical treatment offers more insight.

4 ANALYTICAL TREATMENT

4.1 Resonances and Tune Modulation

The transverse phase space of HERA is covered by a web of weak, isolated resonance islands. Close to one of these resonances, $kQ_x + lQ_z \approx p$, the transverse motion is well described by the nonlinear Hamiltonian

$$H(I_x, I_z, \phi_x, \phi_z, \theta) = I_x Q_{x0} + I_z Q_{z0} + g(I_x, I_z) +$$
$$+h(I_x, I_z) \cos(k\phi_x + l\phi_z - p\theta) +$$
$$+q \cdot (I_x + I_z) \cdot \cos(Q_m \theta + \alpha), \qquad (4)$$

where the last term represents a tune modulation of amplitude q and frequency Q_m in both transverse planes and α an initial phase. The terms I_x and I_z designate the horizontal and vertical action, respectively; ϕ_x and ϕ_z are the corresponding angle variables; and θ denotes the azimuthal position around the storage ring. The function h is called driving term. It determines the strength of the resonance and, for HERA, is typically much smaller than the detuning term g [1].

Differential-algebra methods in conjunction with normal-form algorithms [11] provide an efficient way to compute the Hamiltonian (4). Care has to be taken, however, since resonances of order lower than 11 may cause a divergence of the normal-form transformation. One possible approach [1] is to first perform an eighth order normal-
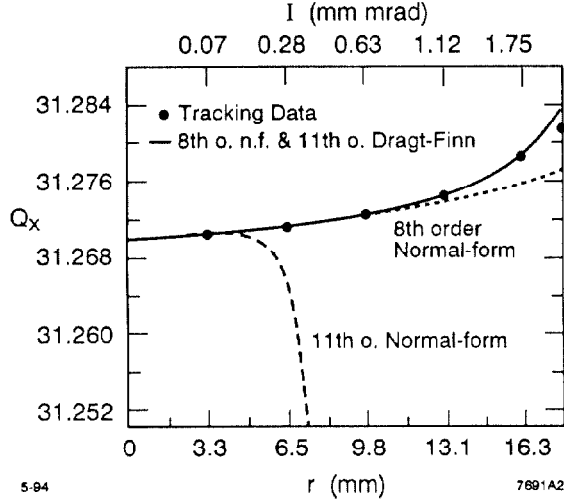
Figure 2: Horizontal tune Q_x obtained from tracking and from different normalization schemes as a function of amplitude $r \equiv (2\beta I_x)^{\frac{1}{2}}$, ($\beta = 76$ m, $I_z = 0$).

ization and then to rewrite the remainder as a Dragt-Finn factorization [12]. The original map M, extracted from the HERA model, is then cast into the following form:

$$M = A^{-1} e^{:-2\pi Q I + t_3(I) + \ldots + t_8(I):} e^{:f_9(I,\phi):} \ldots$$
$$\ldots e^{:f_{11}(I,\phi):} A + \mathcal{O}(12), \tag{5}$$

where the t_n and f_n are polynomials of degree n in $y = \sqrt{2I_y} \cos\phi_y$, and $p_y = -\sqrt{2I_y} \sin\phi_y$ ($y = x, z$). The A denotes the eighth order normal-form transformation. The tunes are given by the first partial derivatives with respect to $I_{x,z}$ of the approximate Hamiltonian

$$H_{\text{approx}} = A^{-1}[QI - \frac{1}{2\pi}\{t_3(I) + \ldots + t_8(I) +$$
$$+ < f_9(I,\phi) + \ldots + f_{11}(I,\phi) >_\phi\}]. \tag{6}$$

Here, the angular brackets indicate an average over $\phi_{x,z}$. Tune curves obtained by this method and those from an eighth and an eleventh order normal-form analysis are compared with the tracking data in Fig. 2. The divergence of the eleventh order normal-form analysis and the shortcoming of an eighth order normalization are evident, while the combination of a normal-form transformation and a Dragt-Finn factorization reproduces the amplitude-dependent tunes up to the threshold of chaotic motion found in the simulations without tune modulation.

To identify the relevant high-order resonances the amplitude-dependent tunes are depicted for three different working points in Fig. 3. It is possible to identify 28 resonances of order 7 to 11, which are crossed by the tune, if the starting action is changed continuously from 0 to 2 mm mrad along the three lines $I_x = 0$, $I_z = 0$, and $I_x = I_z$. In the following, we will use this set of resonances [1] to determine typical values of certain quantities.

The Hamiltonian (4), whose contour lines form an island structure in phase space, can be further approximated by a nonlinear pendulum [13]. The pendulum motion is characterized by two parameters: the island width ΔI_{tot} and
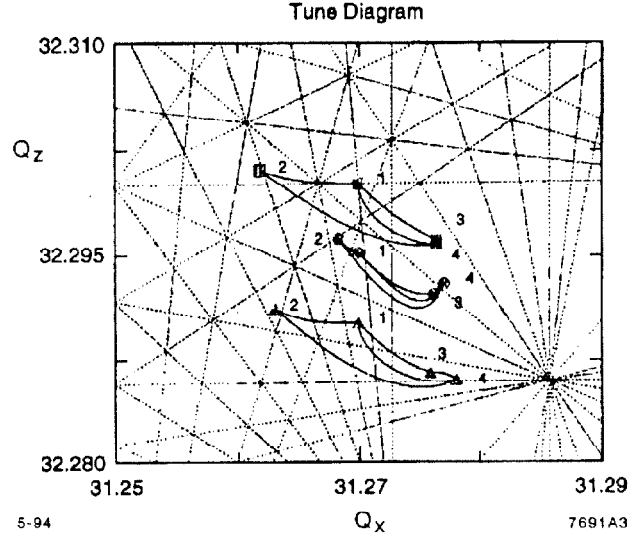

Figure 3: Diagram of the amplitude-dependent particle tunes and of all resonance lines up to order 11. The numbered dots indicate tunes for special values of the starting actions, $(I_x, I_z)=$ 1) (0,0); 2) (0,2); 3) (2,0); 4) (2,2), in units of mm mrad. The connecting lines correspond to a continuous variation of the initial action between these values. The squares, circles, and triangles refer to three different working points.
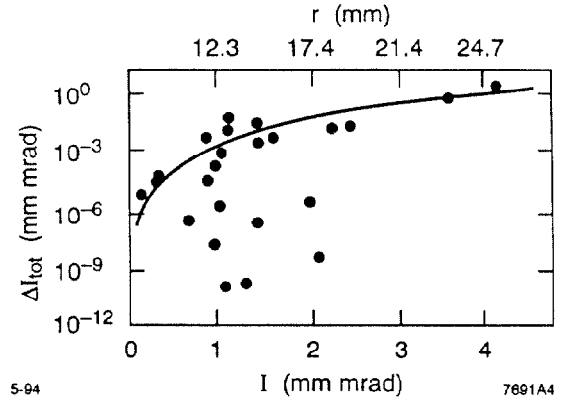

Figure 4: Total island width ΔI_{tot} as a function of the resonant action $I \equiv I_x + I_z$. The curve represents the parametrization $\Delta I_{tot} \approx 2.4 \cdot 10^{-3} I^4 (\text{mm mrad})^{-3}$.

the island tune Q_I. The former describes the size of the island in action space $\Delta I_{\text{tot}} \equiv (\Delta I_x^2 + \Delta I_z^2)^{\frac{1}{2}}$ and reads

$$\Delta I_{\text{tot}} = 4 \left(\frac{(l^2 + k^2)h}{|l^2 \frac{\partial^2 g}{\partial I_z^2} + 2kl \frac{\partial^2 g}{\partial I_z \partial I_x} + k^2 \frac{\partial^2 g}{\partial I_x^2}|} \right)^{\frac{1}{2}}. \tag{7}$$

Figure 4 shows the island width ΔI_{tot} for the above set of high-order resonances. Note that the resonances represented in the picture are encountered for different working points and along different lines in tune space and that a typical separation of resonances along one line is 0.5–1 mm mrad, so that the resonance overlap criterion [13] is fulfilled only for $I \geq 4$ mm mrad (or $r \geq 25$ mm).

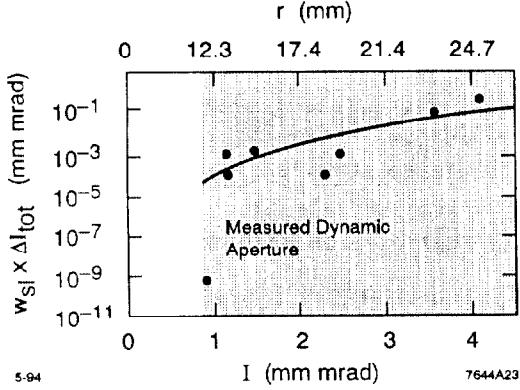The second parameter—the island tune Q_I—designates the frequency at which particles inside a resonance island

Figure 5: Absolute width of stochastic layer $\Delta I_{tot} \cdot w_{sl}$ as a function of the resonant action $I \equiv I_x + I_z$. A tune modulation amplitude of $q \sim 5 \cdot 10^{-5}$ at a frequency of 50 Hz is assumed. The curve represents the parametrization $w_{sl} \cdot \Delta I_{tot} \approx 10^{-4} I^5 (\text{mm mrad})^{-4}$.

oscillate around the elliptic fixed point [14]. It is given by

$$Q_I = \left[k^2 \frac{\partial^2 g}{\partial I_x^2} + 2kl \frac{\partial^2 g}{\partial I_x \partial I_z} + l^2 \frac{\partial^2 g}{\partial I_z^2} \right]^{\frac{1}{2}} h^{\frac{1}{2}}, \qquad (8)$$

evaluated at the resonance. The island tune for resonances through order 11 varies between $3 \cdot 10^{-15}$ (10^{-10} Hz) at very small amplitudes and $5 \cdot 10^{-4}$ (25 Hz) for amplitudes of about 23 mm ($\beta = 76$ m) [1]. Resonance islands are most sensitive to an external tune modulation at frequencies close to the island frequency. In contrast, they are almost undisturbed by high-frequency perturbations (i.e., $f > 100$ Hz). The fraction of the resonance island w_{sl} which becomes chaotic under the influence of a tune modulation of amplitude q and frequency Q_m can be derived explicitly and, within a factor of 2, is given by [13, 1]

$$w_{sl} \approx \pi |k + l| q Q_m^2 / \left(2Q_I^3 \cosh\left(\pi Q_m/2Q_I\right) \right). \qquad (9)$$

In Fig. 5 the absolute width of the chaotic layer $w_{sl} \Delta I_{tot}$ is depicted for each resonance, again as a function of the action I. Comparison with Fig. 4 shows that up to 10% of a resonance island can become chaotic. For about half of the resonances of Fig. 4, however, the stochastic width is insignificant. In particular, it is negligibly small at resonant action values below $I_0 \approx 0.8$ mm mrad ($r \approx 11$ mm). This I_0 approximates the threshold for tune-modulation induced diffusion, independently of the exact details of the diffusion mechanism, and its value is in remarkable agreement with the dynamic acceptance measured.

4.2 Diffusion Rates

A concept complementary to the dynamic aperture is the amplitude-dependent diffusion rate, which is very important for background considerations and for experiments in the beam halo. A possible semi-analytical scheme for evaluating macroscopic (i.e., measurable) diffusion rates contains the following basic ingredients:

1. the parameters of isolated, high-order resonances,

2. local diffusion rates in the vicinity of a single resonance, and

3. a method to combine the local diffusion rates at each resonance into a macroscopic 'global' diffusion rate, which may be compared with measurements.

A diffusion equation was successfully applied to parametrize the beam profile evolution in the Fermilab Tevatron [15] and is routinely employed to analyze the transverse drift rates measured with the HERA collimator system [16]. A diffusion equation for the total transverse action $I \equiv I_x + I_z$ is of the form

$$\partial f/\partial t = \partial/\partial I \cdot \left(D(I)\partial f/\partial I\right), \qquad (10)$$

where f denotes the distribution function. The diffusion coefficient $D(I)$ is related to the squared action change per time interval by the formula [1]

$$D(I) = \left\langle \overline{(\Delta I)^2}/(2\Delta t) \right\rangle. \qquad (11)$$

Here, the bar indicates the mean over a particle ensemble. An approach to calculating the 'global' diffusion coefficient $D(I)$ consists of averaging the local diffusion rates describing motion close to a single resonance over the region between two adjacent resonances. This average, indicated by the angular brackets in (11), can be motivated by a continuous slow drift of resonance islands in phase space. Several mechanisms can cause a local diffusion of particles:

a. The effect of an external diffusion (for instance gas scattering) can be considerably increased in the vicinity of a resonance if the resonance island and the island tune are sufficiently large and if the angle in action space between energy surface and resonance contour is small. The enhanced diffusion is known as *resonance streaming* [17, 18].

b. Particles inside the thin stochastic layer which is generated by tune modulation around the separatrix of a primary resonance may diffuse *along* the resonance contour under the influence of a second resonance, which is an example of *Arnold diffusion* [13, 18].

c. If the machine parameters were kept constant, the strong diffusion of particles *across* the chaotic layer would have no measurable effect. Since the tunes change continuously, however, the resonance islands are altering their position in the four dimensional phase space, and individual particles will follow a succession of regular and chaotic trajectory segments. A measurable diffusion rate called *sweeping diffusion* is the result [2].

d. A tune modulation of small modulation frequency Q_m and large amplitude q generates a strongly chaotic band of overlapping sideband resonances. Particles inside this 'modulational layer' can be driven *along* the resonance contour by another resonance. This mechanism is known as *modulation diffusion* [19, 18].
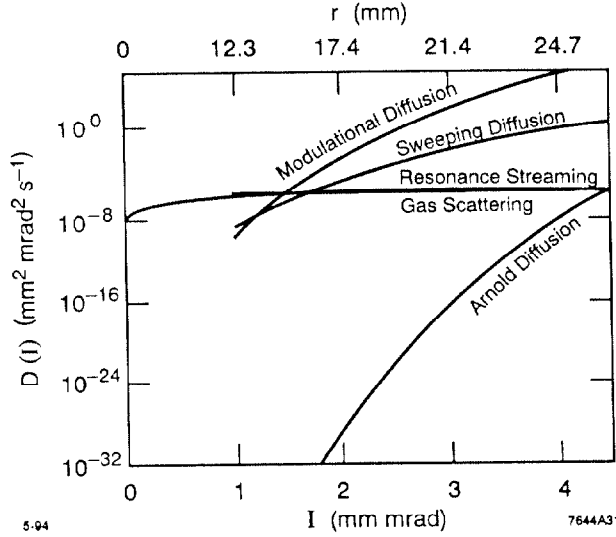
330

Figure 6: Comparison of diffusion coefficients computed for different types of nonlinear transport mechanisms and for gas scattering ($p_{H_2} = 2 \cdot 10^{-9}$ mbar) as a function of action [2].

The diffusion processes a–d are locally described by a Fokker-Planck equation in the action variable [18, 17, 13, 19, 2]. If the motion is Hamiltonian, the Fokker-Planck equation reduces to a diffusion equation with action-dependent coefficients [18, 1]. Thus, it is not too surprising that a diffusion equation also parametrizes the macroscopic behavior as reflected in beam profile and background.

Figure 6 compares the relative significance of different diffusion processes [2]. The figure shows that modulational diffusion is the dominant transport process and that its associated diffusion rate exhibits a steep increase as a function of amplitude. The latter was calculated assuming that the particles are driven along the modulational layer under the action of the linear coupling resonance $Q_x - Q_z = -1$,

$$H_{coupl}(I_x, I_z) = \kappa I_x^{\frac{1}{2}} I_z^{\frac{1}{2}} \cos(\phi_x - \phi_z + \theta + \chi_0), \qquad (12)$$

where the parameter $\kappa \approx 0.005$ corresponds to the minimum distance of the measured tunes as a function of nominal tunes [21], and χ_0 is an initial phase.

The estimated diffusion rate agrees qualitatively with the observation, but is too small by six or seven orders of magnitude to explain the measured dynamic aperture. This discrepancy may be ascribed to resonances of order higher than 11, omitted in the analytical calculation, or to a diffusion mechanism different from those considered here.

5 SUMMARY AND CONCLUSIONS

For tracking calculations and analytical studies a very detailed model of the HERA proton ring is available, which includes the measured field errors up to 20-poles for each individual magnet.' The dynamic aperture predicted by simulations and the measured value agree within a factor

of 2. A better agreement is achieved if the effect of tune modulation is also considered: for a realistic tune modulation, chaotic trajectories are theoretically expected, and indeed are observed in the simulation, at amplitudes very close to the actual dynamic aperture. The dynamic aperture in HERA appears to be caused by the combined effects of nonlinear field errors, tune modulation, and drifting machine parameters.

6 ACKNOWLEDGEMENTS

7 REFERENCES

[1] F. Zimmermann, DESY 93–59 (1993).

[2] F. Zimmermann, SLAC–PUB–6458 (1994); and "Transverse Proton Diffusion," submitted to Part. Acc. (1994).

[3] F. Willeke and F. Zimmermann, Proc. IEEE PAC, San Francisco (1991) p. 2483; S. Herb et al., Proc. 1992 HEACC, Hamburg (1992) p. 398.

[4] C. Daum et al., DESY HERA 89–09 (1989).

[5] H. Brück, R. Meinke, F. Müller, and P. Schmüser, DESY 89–041 (1989); R. Brinkmann and F. Willeke, DESY HERA 88–08 (1988).

[6] A. Wrulich, DESY 84-026 (1984); F. Schmidt, CERN SL/90–52 (AP) (1991).

[7] F. Schmidt, F. Zimmermann, and F. Willeke, Part. Acc. 35 (1991) 249.

[8] M. Hénon and C. Heiles, Astron. J. 69 (1964) 73, V.I. Oseledec, Trans. Moscow Math. Soc. 19 (1968) 197; G. Benettin et al., Meccanica 15, 9, 21 (1980).

[9] K. Wittenburg, Proc. EPAC 92, Berlin (1992) p. 1133.

[10] H. Brück et al., Proc. EPAC 90, Nice (1990) p. 329.

[11] M. Berz, Part. Acc. 24 (1989) 109; É. Forest, M. Berz, and J. Irwin, Part. Acc. 24 (1989) 91.

[12] A. J. Dragt and J. M. Finn, J. Math. Phys. 17 (1976) 2215–2227.

[13] B. V. Chirikov, Physics Reports 52, No 5 (1979).

[14] T. Chen and S. Peggs, Proc. 3rd ICFA beam dynamics workshop, Novosibirsk (1989).

[15] T. Chen et al., Phys. Rev. Lett. 68 (1992) 33.

[16] M. Seidel, DESY HERA 93–04 (1993).

[17] J. Tennyson, Physica 5D (1982) 123–135; A. Gerasimov, Proc. IEEE PAC, San Francisco (1991) p. 1678.

[18] A. J. Lichtenberg, M. A. Lieberman, Regular and Stochastic Motion, Springer Verlag (1983).

[19] B. V. Chirikov, M. A. Lieberman, D. L. Shepelyansky, and F. M. Vivaldi, Physica 14D (1985) 289-304.

[20] A. Schoch, CERN 57–21 (1958) pp. 55–56; L. R. Evans and J. Gareyte, CERN SPS/82–8 (DI-MST) (1982); L. R. Evans, in CERN 84–15 (1984).

[21] G. Ripken, F. Willeke, DESY 88-114 (1988).